

Motion of discrete solitons assisted by nonlinearity management

Jesús Cuevas¹, Boris A. Malomed² and P.G. Kevrekidis³

¹ *Grupo de Física No Lineal, Departamento de Física Aplicada I, Escuela Universitaria Politécnica, C/ Virgen de África, 7, 41011 Sevilla, Spain*

² *Department of Interdisciplinary Studies, School of Electrical Engineering, Faculty of Engineering, Tel Aviv University, Tel Aviv 69978, Israel*

³ *Department of Mathematics and Statistics, University of Massachusetts, Amherst MA 01003-4515, USA*

(Dated: June 14, 2018)

We demonstrate that periodic modulation of the nonlinearity coefficient in the discrete nonlinear Schrödinger (DNLS) equation can strongly facilitate creation of traveling solitons in the lattice. We predict this possibility in an analytical form, and test it in direct simulations. Systematic simulations reveal several generic dynamical regimes, depending on the amplitude and frequency of the time modulation, and on initial thrust which sets the soliton in motion. These regimes include irregular motion, regular motion of a decaying soliton, and regular motion of a stable one. The motion may occur in both the straight and reverse directions, relative to the initial thrust. In the case of stable motion, extremely long simulations in a lattice with periodic boundary conditions demonstrate that the soliton keeps moving as long as we can monitor without any visible loss. Velocities of moving stable solitons are in good agreement with the analytical prediction, which is based on requiring a resonance between the ac drive and motion of the soliton through the periodic potential. All the generic dynamical regimes are mapped in the model's parameter space. Collisions between moving stable solitons are briefly investigated too, with a conclusion that two different outcomes are possible: elastic bounce, or bounce with mass transfer from one soliton to the other. The model can be realized experimentally in a Bose-Einstein condensate trapped in a deep optical lattice.

I. INTRODUCTION

The discrete nonlinear Schrödinger (DNLS) equation is a well-known fundamental model of nonlinear lattice dynamics, which allows to study many features of the nonintegrable dynamics in the universal setting [1]. Simultaneously, this model finds direct applications to arrays of nonlinear optical waveguides (as it was predicted long ago [2] and demonstrated in detail more recently, see Refs. [3] and references therein), and to arrays of droplets in Bose-Einstein condensates (BECs) trapped in a very deep optical lattice [4].

In all these contexts, discrete solitons are the most fundamental dynamical excitations supported by the DNLS equation. The dynamics of standing solitons, pinned by the underlying lattice, is understood quite well, in terms of both numerical simulations and analytical approximations, the most general one being based on the variational method [5]. However, moving discrete solitons is a more complex issue [6, 7]. While, strictly speaking, exact solutions for moving solitons should not exist because of the radiation loss, direct simulations indicate that a soliton may move freely if its “mass” (l^2 norm) does not exceed a certain critical value [7]. In the quasi-continuum approximation, the source of the braking force acting on the moving soliton is the effective Peierls-Nabarro (PN) potential induced by the lattice [8].

In the case of the DNLS equation describing an array of nearly isolated droplets of a BEC in a deep optical lattice, an interesting possibility is to apply the *ac Feshbach-resonance management* (FRM) to it, as it was recently proposed in Ref. [9]. FRM may be induced by an external ac magnetic field, which periodically (in time) changes the sign of the nonlinearity by dint of the FR affecting collisions between atoms (for a one-dimensional BEC without the optical lattice, the concept of FRM was proposed in Ref. [10]).

In this work, our aim is to demonstrate that the FRM, applied to the DNLS model, can strongly facilitate the motion of discrete solitons (Ref. [9] was only dealing with standing solitons). The model is based on the equation

$$i\dot{u}_n + u_{n+1} + u_{n-1} - 2u_n + g(t)|u_n|^2 u_n = 0, \quad (1)$$

where $u_n(t)$ are the mean-field BEC wave functions at the lattice sites, and the real time-dependent nonlinear coefficient, proportional to the scattering length, is

$$g(t) = g_{dc} + g_{ac} \sin(\omega t). \quad (2)$$

Our presentation will be structured as follows: In section II, approximating the soliton by a *Gaussian*, we present an analytical estimate of the effective PN potential for the *moving* discrete soliton. The estimate suggests that the ac

modulation of $g(t)$ may indeed help to suppress the PN potential, and thus facilitate free motion of discrete solitons. In section III, we display results of systematic simulations, summarized in the form of diagrams in the parameter plane (ω, g_{ac}) . The diagrams feature several generic dynamical regimes, including a large area of stable progressive motion, that can last indefinitely long. Collisions between solitons moving in opposite directions are briefly considered too, with a conclusion that they bounce from each other, sometimes featuring mass transfer between the solitons. Diverse dynamical regimes predicted in this work suggest straightforward possibilities for new experiments in the BEC trapped in a deep optical lattice. Finally, in section IV, we summarize our findings and present our conclusions.

II. ANALYTICAL APPROXIMATION

The continuum limit suggests the following *ansatz* for a moving soliton [11],

$$u_{\text{ans}}(n, t) = A \exp \left[-a(n - \xi(t))^2 + i\phi(t) + (i/2)\dot{\xi}n - (i/4) \int (\dot{\xi}(t))^2 dt \right], \quad (3)$$

where A , a , $\xi(t)$, and ϕ are, respectively, the amplitude, squared inverse width, central coordinate, and phase of the soliton. Accordingly, $\dot{\xi}$ is the soliton's velocity, $\dot{\xi}/2$ simultaneously being the wavenumber of the wave field carrying the moving soliton. For the true soliton, in the continuum limit, the variational approximation yields the following relations:

$$\dot{\phi} = 3a, \quad A^2 = 4\sqrt{2}a/g, \quad (4)$$

if $g = \text{const} > 0$. In Eqs. (4), a is regarded as an arbitrary positive constant (intrinsic parameter of the soliton family).

To estimate the PN potential acting on the *quasi-continuum* soliton in the *discrete* system, we use the Hamiltonian corresponding to the DNLS equation (1),

$$H = \sum_{n=-\infty}^{+\infty} \left[2|u_n|^2 - (u_n^* u_{n+1} + u_n u_{n+1}^*) - \frac{g}{2} |u_n|^4 \right], \quad (5)$$

the asterisk standing for the complex conjugation. Substituting the *ansatz* (3) into H , the potential of the soliton-lattice interaction can be calculated in the form of a Fourier series, $H(\xi, \dot{\xi}) = \sum_{m=0}^{\infty} H_m(\dot{\xi}) \cos(2\pi m\xi)$. In the case of a broad soliton, for which the *ansatz* (3) is relevant, we keep only the lowest harmonic ($m = 1$), which is actually the PN potential U_{PN} . After some simple algebra, we thus find

$$U_{\text{PN}}(\xi, \dot{\xi}) = \frac{1}{2} \sqrt{\frac{\pi}{a}} A^2 \exp\left(-\frac{\pi^2}{4a}\right) \left\{ 4\sqrt{2} \exp\left(-\frac{\pi^2}{4a}\right) \left[1 + e^{-a/2} \cos\left(\dot{\xi}/2\right) \right] - gA^2 \sqrt{\frac{\pi}{a}} \right\} \cos(2\pi\xi). \quad (6)$$

A novel feature in this estimate, in comparison with known perturbative results [8], is the dependence on the soliton's velocity, $\dot{\xi}$.

If the soliton's relation between a and A^2 , as given by Eq. (4) (for constant g), is substituted in Eq. (6), the coefficient in front of $\cos(2\pi\xi)$, i.e., the amplitude of the PN potential, never vanishes. However, it may vanish if the underlying pulse (3) is considered not as a soliton, but just as a pulse with A^2 and a taken independently; then, the condition of the vanishing of the PN potential determines a *discrete spectrum* of the velocities $\dot{\xi}$, in the form

$$1 + \exp(-a/2) \cos\left(\dot{\xi}/2\right) = (gA^2/4) \sqrt{\pi/(2a)} \exp(\pi^2/(4a)), \quad (7)$$

provided that gA^2 is small enough to make the right-hand side of Eq. (7) smaller than 2 [this caveat is essential, as the factor $\exp(\pi^2/(4a))$ may be exponentially large].

In this work, however, our objective is not to verify this possibility, but rather to consider the case when the nonlinear coefficient g is a function of time, as per Eq. (2). Note that, for a broad soliton (small a), the PN potential barrier is exponentially small, hence the soliton's kinetic energy may be much larger than the potential. This implies that the velocity of the soliton moving through the potential (6) with the period $L = 1$ contains a constant (dc) part and a small ac correction to it, with the frequency $2\pi\dot{\xi}_0/L \equiv 2\pi\dot{\xi}_0$ [12]:

$$\dot{\xi}(t) \approx \dot{\xi}_0 + \dot{\xi}_1 \cos(2\pi\dot{\xi}_0 t), \quad \dot{\xi}_1^2 \ll \dot{\xi}_0^2. \quad (8)$$

Then, the substitution of the expression (8) into the condition (7), which provides for the suppression of the PN potential, one can expand its left-hand side,

$$1 + \exp(-a/2) \cos(\dot{\xi}/2) \approx 1 + \exp(-a/2) \left[\cos(\dot{\xi}_0/2) - (\dot{\xi}_1/2) \sin(\dot{\xi}_0/2) \cos(2\pi\dot{\xi}_0 t) \right]. \quad (9)$$

Now, substituting the variable $g(t)$ from Eq. (2) into the right-hand side of Eq. (7), it is obvious that g_{dc} and g_{ac} can be chosen so as to provide for the fulfilment of the condition, provided that the average soliton's velocity takes the *resonant value*, $\dot{\xi}_0 = \omega/2\pi$. More generally, due to anharmonic effects, one may expect the existence of a spectrum of resonant velocities,

$$\dot{\xi}_0 = (c_{res})_N^{(M)} \equiv M\omega/2\pi N, \quad (10)$$

with integers M and N .

Actually, an ac drive can support stable progressive motion of solitons at the resonant velocities (10) (assuming the spatial period $L = 1$), even in the presence of dissipation, in a broad class of systems. This effect was first predicted for discrete systems (of the Toda-lattice and Frenkel-Kontorova types) in Refs. [13], and demonstrated experimentally in an LC electric transmission line in Ref. [14]. Later, the same effect was predicted [15] and demonstrated experimentally [16] in continuous long Josephson junctions with a spatially periodic inhomogeneity. All of the above examples were in the context topological (kink-like) excitations in the aforementioned models. The only example similar to what is suggested here in the context of *non-topological solitons* that we are aware of, was in the work of [17] (the context in the latter case involved damping and external, fixed and localized in space ac-drive). Note also that the mechanism of the ac-driven motion considered here is different from that in ratchet systems (see, e.g., Ref. [18] and references therein).

III. NUMERICAL RESULTS

We now proceed to examine the above analytical predictions through direct numerical simulations. We integrate Eq. (1) with an initial configuration in the form of a standing-soliton solution for the case of $g_{ac} = 0$. This solution has the form of $u_n(t) = v_n \exp(i\nu t)$, with the real field v_n obeying the equation

$$\nu v_n = v_{n+1} + v_{n-1} - 2v_n + g_{dc} v_n^3. \quad (11)$$

Equation (11) was solved by means of well-known methods (starting from the anti-continuum limit). Then, to set the soliton in motion, it was provided with a lattice momentum q , so that the initial condition was

$$u_n(0) = v_n \exp(inq/2). \quad (12)$$

Equation (12) implies that the soliton will move to the right if $q > 0$.

The results will be displayed for $g_{dc} = 1$, $\nu = 1$, and three values of the initial thrust, $q = 0.25$, $q = 0.5$ and $q = 1$, as these cases were found to represent a generic situation in the plane of the ac-drive's parameters (ω, g_{ac}). Simulations were run in the interval $0 < t < 100 \times (2\pi/\omega)$ or longer, by means of the fourth-order Runge-Kutta algorithm, with the time step $\Delta t = 0.002$. In most cases, the lattice with 251 sites was used. Edge absorbers were installed by adding the loss term $i\gamma u_n$, with $\gamma = 1$, to Eq. (1) at the ten sites adjacent to each edge. Besides that, extremely long simulations were performed in a longer lattice with periodic boundary conditions, to verify if the motion could last for very long times, and also to examine collisions between the solitons, see below.

If $g_{ac} = 0$, the soliton pushed as per Eq. (12) with $q \lesssim 0.7$ does not move. Instead, it remains pinned to the lattice, with its center oscillating around an equilibrium position. This observation may be explained by the fact that the kinetic energy given to the soliton is smaller than the height of the PN potential barrier.

Several distinct types of the dynamics were observed at $g_{ac} > 0$, depending on the driving frequency ω and the thrust parameter q . First, the soliton may remain pinned, as shown in Fig. 1. In this case, the simulations [run in the interval $0 < t < 300 \times (2\pi/\omega)$] demonstrate that the soliton stays pinned within a few sites from its initial position. The central coordinate and ‘‘participation number’’ P (actually, it measures an average width of the soliton), shown in Fig. 1 and elsewhere, are defined as

$$X = \sum_n n |u_n|^2 / \sum_n |u_n|^2, \quad P = \left(\sum_n |u_n|^2 \right)^2 / \sum_n |u_n|^4. \quad (13)$$

The next generic regime is that of irregular motion, as shown in Fig. 2. A characteristic feature of this regime is that the soliton randomly changes the direction of motion several times, and the velocity remains very small in comparison with regimes of “true motion”, see below.

Under the action of a stronger drive, the soliton can also split into two secondary ones moving in opposite directions, see Fig. 3. As is seen, the splitting is strongly asymmetric, and the heavier secondary soliton (splinter) may move both forward and backward, with respect to the initial push. We notice that splitting of a *quiescent* soliton (without any initial thrust applied to it) into two *symmetric* splinters, moving in opposite directions with equal velocities, was reported, in the same model based on Eq. (1), in Ref. [9]. The initial push applied to the soliton is a natural cause for the symmetry breaking observed here in the case of the splitting.

Two distinct regimes of regular motion of the soliton were also observed. In one case, shown in Figs. 4 and 5, the moving soliton is not really stable, as it gradually decays into radiation. The most interesting case is that of persistent *stable motion* of the soliton, without any observable decay (after an initial transient stage of the evolution). Examples of the latter are displayed in Figs. 6 and 7. To distinguish between the two different regimes of free motion, we have adopted a criterion that the moving soliton is stable if it keeps more than 70% of the mass, $\sum |u_n|^2$, in its core. While this criterion entails a degree of arbitrariness, we have found that it accurately represents the dynamics of the structures resulting from the FRM. The generic examples displayed in Figs. 4 - 7 demonstrate that free motion of the soliton is possible in both the straight and reverse directions, relative to the initial thrust.

As stable motion of solitons in the nonintegrable discrete model is an issue of obvious interest, we have further investigated this case, replacing the finite lattice with edge absorbers by a ring-shaped one, with periodic boundary conditions. This setting opens a way to study indefinitely long motion of the soliton. The result, illustrated by examples shown in Fig. 8, is that the moving solitons remains stable (preserving its shape) as long as the simulations could be run. In this case, it is natural to compare the average velocity \bar{c} of the persistent motion with the prediction given by Eq. (10). The result is $\bar{c}_1 \approx 0.246$ and $\bar{c}_2 \approx 0.155$ in the cases shown in Figs. 8(a) and Fig. 8(b), respectively. Comparison with the analytical formula (10) (with $\omega = 1$, which is the driving frequency in the examples shown in Fig. 8) demonstrate that \bar{c}_2 and \bar{c}_1 fit well to the predicted values in the cases of the, respectively, fundamental and second-order resonance,

$$\bar{c}_2 / (c_{\text{res}})_1^{(1)} \approx 0.974, \bar{c}_1 / (c_{\text{res}})_3^{(2)} \approx 1.029 \quad (14)$$

Relatively small discrepancies between the predicted and observed values in Eq. (14) can be explained by the fact that the effective perturbations are not really weak in these cases.

For the fixed values of $g_{\text{dc}} = 1$ in Eq. (2) and $\nu = 1$ in Eq. (12), and several values of the initial thrust in Eq. (initial), $q = 0.25, 0.5$, and 1, we have collected results of systematic simulations, varying the drive’s parameters, g_{ac} and ω , by small steps in broad ranges spanning the relevant two-parameter space. The results are encompassed in Fig. 9, in the form of maps in the (ω, g_{ac}) plane, where we outline regions giving rise to each of the qualitatively different dynamical regimes described above. This road map is one of the key findings of the present work, detailing the various possibilities arising as a result of FRM in a dynamical lattice.

Some general features can be deduced from examination of the maps in Fig. 9. As is seen, the increase of the initial thrust q significantly affects the map, although quantitatively, rather than qualitatively. At all values of q , the irregular motion is, generally, changed by stable progressive motion (straight or reverse) with the increase of the drive’s amplitude, and/or decrease of its frequency, which seems quite natural. Further increase of the drive’s strength, which implies the applications of a relatively strong perturbation to the system, may be expected to lead to an instability, which indeed happens, in the form of an onset of the gradual decay of the moving solitons. Finally, strong instability sets in, manifesting itself in the splitting of the soliton. It also seems natural that the soliton is more prone to splitting if the driving frequency is low, as internal strain in the pulse, which eventually leads to its splitting, has more time to accumulate if the drive oscillates slowly.

Transition to the reverse motion tends to happen parallel to the transition from the stable moving soliton to the decaying one. For this reason, in most cases (but not always) backward-moving soliton are decaying ones. Finally, it should be noted that the increase of the initial thrust leads to overall *stabilization* of the soliton (somewhat counter-intuitively), making the decay and splitting zones smaller.

Finally, using the large lattice with the periodic boundary conditions, we also simulated collisions between solitons originally moving with opposite velocities. Initial pulses were generated by applying the thrust $\pm q$ to two quiescent solitons. A systematic study of collisions is very difficult in the present model, cf. Ref. [7]. Nevertheless, we were able to identify two different types of the interaction, typical examples of which are shown in in Fig. 10.

In the case of Fig. 10(a), the solitons bounce back from each other quite elastically. Afterwards, one of the soliton spontaneously reverses its direction of motion, due to its interaction with the underlying lattice. Eventually, we observe a pair of virtually noninteracting solitons traveling indefinitely long in the same direction.

In another case, Fig. 10(b), the solitons also bounce after the first collision; however, in this case the collisions are inelastic, resulting in transfer of mass from one soliton to the other. Repeated collisions lead to additional transfer,

and eventually the weak soliton almost disappears.

IV. COCLUSIONS

In this work, we have investigated moving solitons in the DNLS equation with a periodically time-modulated nonlinear coefficient. An approximate analytical consideration predicts that the ac nonlinearity management may facilitate creation of traveling solitons in the lattice. Systematic simulations reveal several generic dynamical regimes, depending on parameters of the time modulation, and the initial thrust which sets the soliton in motion. Besides the possibility that the soliton remains pinned, the basic dynamical regimes feature irregular motion, regular motion of a decaying soliton, and regular motion of a stable one. In the latter case, extremely long simulations in the lattice with periodic boundary conditions demonstrate that the soliton keeps moving indefinitely long without any tangible loss. Velocities of the moving stable solitons are found to be in good agreement with the analytical prediction through a resonance condition, revealing the key mechanism for sustaining the travelling motion. All the generic dynamical regimes were mapped in the model's parameter space. Collisions between stable moving solitons were briefly investigated too, with a conclusion that two different outcomes are possible: elastic bounce, and bounce with mass transfer from one soliton to the other. The model can be realized in a Bose-Einstein condensate trapped in a deep optical lattice, with the nonlinearity modulation induced by the Feshbach resonance in the ac regime.

It would be interesting to examine similar dynamical scenaria for the effect of FRM on dark solitons, and also to monitor how this phenomenology is modified in higher dimensions. Such studies are currently in progress and will be reported in future publications.

Acknowledgements. This work was partially supported by NSF-DMS-0204585, NSF-CAREER, and the Eppley Foundation for Research (PGK); the Israel Science Foundation grant No. 8006/03 (BAM) and the MECD/FEDER project BMF2003-03015/FISI (JC).

-
- [1] P. G. Kevrekidis, K. Ø. Rasmussen, and A. R. Bishop, *Int. J. Mod. Phys. B* **15**, 2833 (2001).
 - [2] D. N. Christodoulides and R. I. Joseph, *Opt. Lett.* **13**, 794 (1988).
 - [3] U. Peschel, R. Morandotti, J. M. Arnold, J. S. Aitchison, H. S. Eisenberg, Y. Silberberg, T. Pertsch, and F. Lederer, *J. Opt. Soc. Am. B* **19**, 2637 (2002); H. S. Eisenberg, R. Morandotti, Y. Silberberg, J. M. Arnold, G. Pennelli, and J. S. Aitchison, *ibid.* **19**, 2938 (2002).
 - [4] A. Trombettoni and A. Smerzi, *Phys. Rev. Lett.* **86**, 2353 (2001); F. Kh. Abdullaev, B. B. Baizakov, S. A. Darmanyan, V. V. Konotop, and M. Salerno, *Phys. Rev. A* **64**, 043606 (2001); G. L. Alfimov, P. G. Kevrekidis, V. V. Konotop, and M. Salerno, *Phys. Rev. E* **66**, 046608 (2002); A. Smerzi and A. Trombettoni, *Phys. Rev. A* **68**, 023613 (2003); *Chaos* **13**, 766 (2003); N. K. Efremidis and D. N. Christodoulides, *Phys. Rev. A* **67**, 063608 (2003).
 - [5] B. Malomed and M. I. Weinstein, *Phys. Lett. A* **220**, 91 (1996).
 - [6] D. B. Duncan, J. C. Eilbeck, H. Feddersen and J. A. D. Wattis, *Physica D* **68**, 1 (1993); S. Flach, Y. Zolotaryuk and K. Kladko, *Phys. Rev. E* **59**, 6105 (1999); M. J. Ablowitz, Z. H. Musslimani and G. Biondini, *Phys. Rev. E* **65**, 026602 (2002).
 - [7] I. E. Papacharalampous, P. G. Kevrekidis, B. A. Malomed, and D. J. Frantzeskakis, *Phys. Rev. E* **68**, 046604 (2003).
 - [8] Yu. S. Kivshar and B. A. Malomed, *Rev. Mod. Phys.* **61**, 763 (1989); Y. S. Kivshar and D. K. Campbell, *Phys. Rev. E* **48**, 3077 (1993); L. Brizhik, A. Fremko, L. Cruzeiro-Hansson, and Y. Olkhovska, *Phys. Rev. B* **61**, 1129 (2000); P. G. Kevrekidis, I. G. Kevrekidis, A. R. Bishop, and E. S. Titi, *Phys. Rev. E* **65**, 046613 (2002).
 - [9] F. Kh. Abdullaev, E. N. Tsoy, B. A. Malomed, and R. A. Kraenkel, *Phys. Rev. A* **68**, 053606 (2003).
 - [10] P. G. Kevrekidis, G. Theocharis, D. J. Frantzeskakis and B. A. Malomed, *Phys. Rev. Lett.* **90**, 230401 (2003).
 - [11] D. Anderson, *Phys. Rev. A* **27**, 3135 (1983).
 - [12] M. Peyrard and M.D. Kruskal, *Physica D* **14**, 88 (1984).
 - [13] B. A. Malomed, *Phys. Rev. A* **45**, 4097 (1992); L. L. Bonilla and B. A. Malomed, *Phys. Rev. B* **43**, 11539 (1991); T. Kuusela, J. Hietarinta, and B. A. Malomed, *J. Phys. A* **26**, L21 (1993); G. Filatrella and B. A. Malomed, *J. Phys. Cond. Matt.* **11**, 7103 (1999).
 - [14] T. Kuusela, *Chaos Sol. Fract.* **5**, 2419 (1995).
 - [15] G. Filatrella, B. A. Malomed, and R. D. Parmentier, *Phys. Lett. A* **198**, 43 (1995).
 - [16] A. V. Ustinov and B. A. Malomed, *Phys. Rev. B* **64**, 020302 (2001).
 - [17] H.E. Nistazakis, P.G. Kevrekidis, B.A. Malomed, D.J. Frantzeskakis and A.R. Bishop, *Phys. Rev. E* **66**, 015601(R) (2002).
 - [18] A. V. Ustinov, C. Coqui, A. Kemp, Y. Zolotaryuk, and M. Salerno, *Phys. Rev. Lett.* **93**, 087001 (2004).

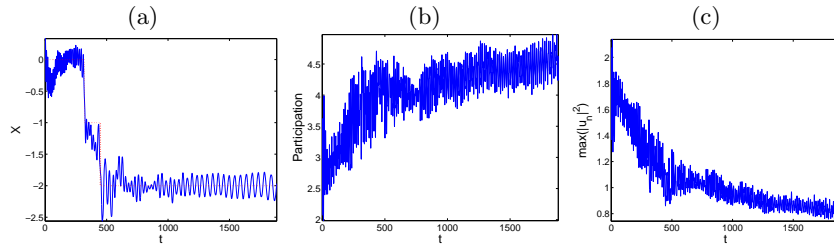


FIG. 1: A typical example of a dynamical regime in which the soliton remains pinned, for $g_{ac} = 0.03$, $\omega = 1$ and $q = 0.5$. Here and in similar plots below, panels display the following variables as functions of time: (a) positions of the center of mass X (red) and maximum X_p (blue) of the density field, $|u_n|^2$; (b) the “participation number” P (which characterizes the width of the soliton); (c) the density amplitude of the soliton, i.e., $|u_n|^2$ at $n = X_p$.

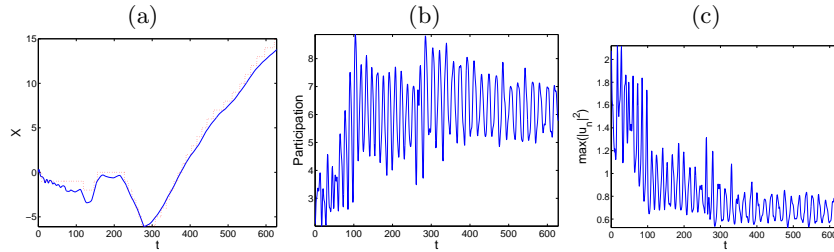


FIG. 2: A generic example of irregular motion of the soliton, for $g_{ac} = 0.065$, $\omega = 1$ and $q = 0.5$.

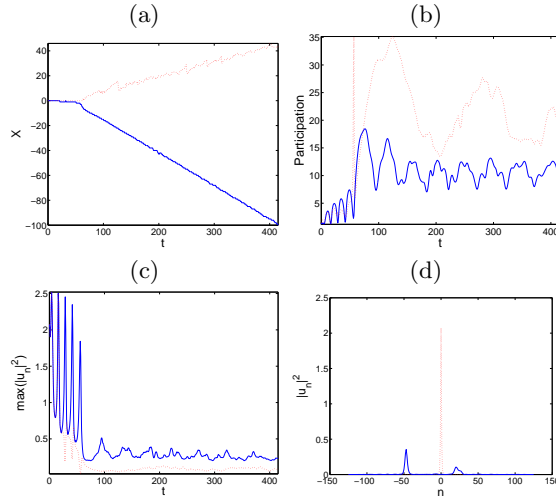


FIG. 3: An example of asymmetric splitting of the soliton, for $g_{ac} = 0.196$, $\omega = 0.5$ and $q = 0.5$. Unlike the previous figures, here panels (a) and (c) show, respectively, the position and magnitude of two local density maxima corresponding to the secondary solitons (splinters) past the splitting point, and panel (b) shows, accordingly, two “participation numbers”, computed as per Eq. (13), but separately for $n \leq 0$ and $n \geq 0$. In this figure and below, an additional panel (d) shows the initial and final density distributions, $|u_n(t=0)|^2$ and $|u_n(t=t_{\text{fin}})|^2$, respectively, by the dashed and continuous lines. In this case, $t_{\text{fin}} = 300$.

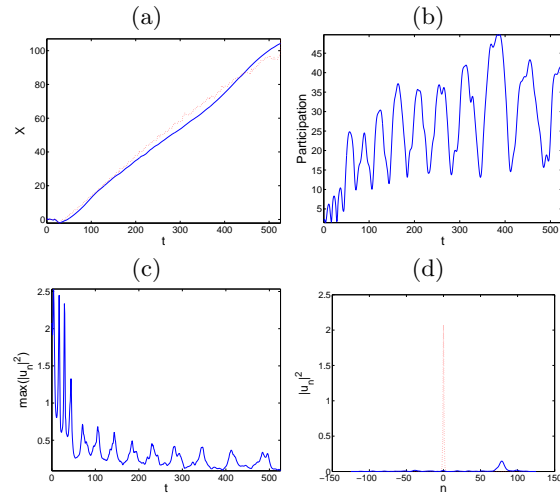


FIG. 4: A generic example of the free motion of a decaying soliton in the straight direction, for $g_{ac} = 0.206$, $\omega = 0.5$ and $q = 0.5$. In panel (d), the final configuration pertains to $t_{\text{fin}} = 400$.

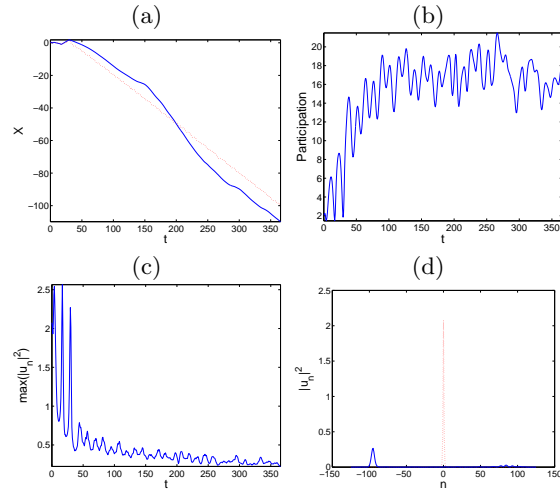


FIG. 5: The same as in Fig. 4, in the case of motion in the reverse direction, for $g_{ac} = 0.218$, $\omega = 0.5$ and $q = 0.5$. In panel (d), the final configuration is shown for $t_{\text{fin}} = 350$.

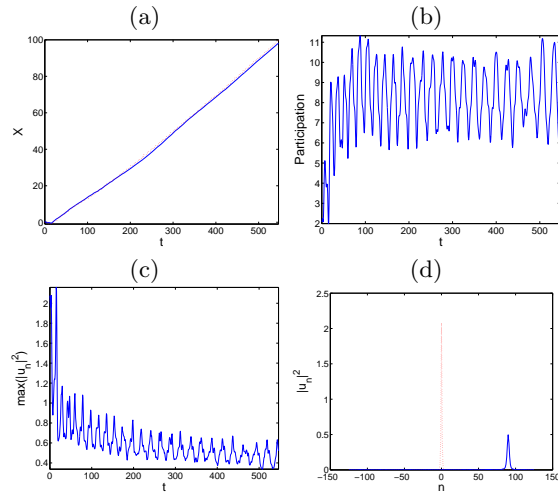


FIG. 6: A generic example of free motion of a *stable* (nondecaying) soliton in the straight direction, for $g_{ac} = 0.132$, $\omega = 1$ and $q = 0.5$. The panel (d) shows the final configuration at $t_{\text{fin}} = 500$.

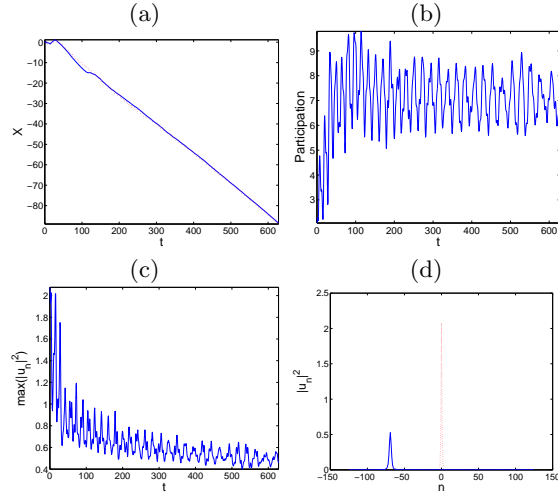


FIG. 7: The same as in Fig. 6, but in the case of motion of a stable soliton in the reverse direction, for $g_{ac} = 0.122$, $\omega = 1$ and $q = 0.5$. The panel (d) shows the final configuration at $t_{\text{fin}} = 500$.

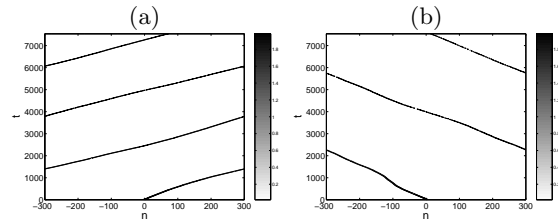


FIG. 8: Indefinitely long motion of stable solitons in a ring lattice composed of 601 sites. The gray-scale plots show the spatiotemporal distribution of the density, $|u_n(t)|^2$. The examples of the straight (a) and inverse (b) motion pertain, respectively, to $g_{ac} = 0.132$, $\omega = 1$, $q = 0.5$, and $g_{ac} = 0.122$, $\omega = 1$, $q = 0.5$.

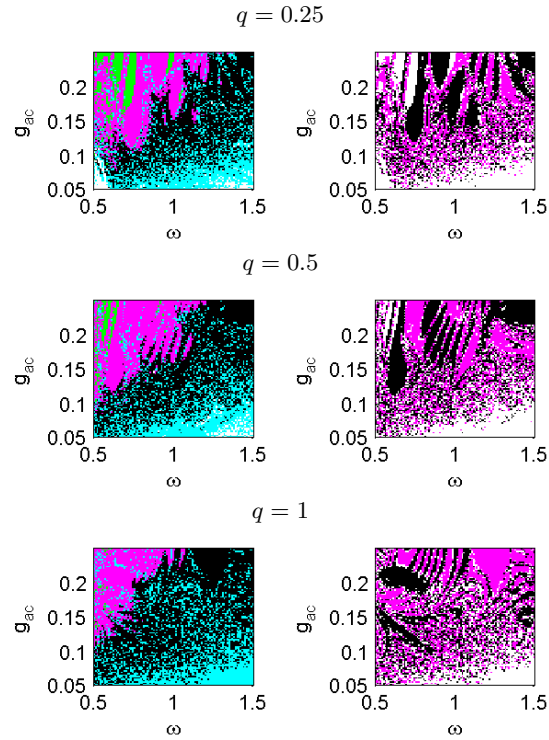


FIG. 9: Maps in the left column show areas in the parameter plane (ω, g_{ac}) which give rise to the following dynamical regimes. White areas: the soliton remains pinned; cyan: irregular motion; green: splitting; magenta: regular motion with decay; black: stable motion (without decay). The maps in the right column additionally show the difference between the forward (alias straight, marked by magenta) and backward (alias reverse, marked by black) directions of the regular motion, relative to the direction singled out by the initial push. Regular-motion regimes for both decaying and stable solitons are included here.

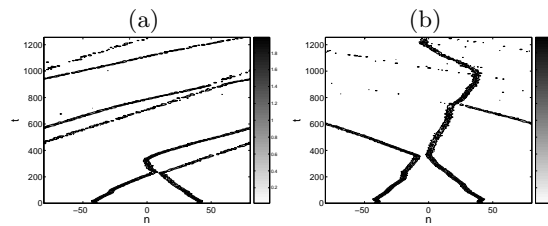


FIG. 10: Two typical examples of different outcomes of collisions between solitons with equal masses moving in opposite directions in the lattice with periodic boundary conditions. The parameters are $g_{ac} = 0.132$, $\omega = 1$, $q = 0.5$ (a) and $g_{ac} = 0.122$, $\omega = 1$, $q = 0.5$ (b). Note that the collision is multiple in panel (b).